Int. J. Electrochem. Sci., 10 **(2015)** 6199 - 6212

International Journal of ELECTROCHEMICAL SCIENCE
www.electrochemsci.org

Effects of Surfactant and Calcining Temperature on Capacitive Properties of Co_3O_4/graphene Compositesfor Supercapacitors

Yanhua Li[1,*], *Shiying Zhang*[1,*], *Qiyuan Chen*[2], *Jingbo Jiang*[2]

[1] Hunan Province Key Laboratory of Applied Environmental Photocatalysis, Changsha University, Changsha 410022, China
[2] College of Chemistry and Chemical Engineering, Central South University, Changsha 410083, China
[*]E-mail: liyanhua11@126.com; cdzhangshiying@163.com

Received: 22 April 2015 / *Accepted:* 25 May 2015 / *Published:* 24 June 2015

Co_3O_4/graphene composites are obtained by hydrothermal synthesis method using different surfactants, followed by calcining precursors at different temperature. XRD and SEM show that different surfactants have a great influence on the crystallite size and the morphology of Co_3O_4 in the composites. The crystallite size of Co_3O_4 in the composites increases with increasing calcining temperature. Electrochemical property displays that the composites prepared in the presence of sodium dodecyl benzene sulfonate (SDBS) surfactant exhibit higher specific capacitancethan those synthesized with addition of Triton X-100 surfactant. Amongall the electrodes, Co_3O_4/GNS-S-350 (Co_3O_4/graphene composites prepared using SDBS and following by calcining precursorsat 350 ℃) electrode exhibits the highest specific capacitance. Its specific capacitancereaches 1033.4 F g^{-1} at 0.2 A g^{-1} and is 3.21 times of that of Co_3O_4/GNS-T-250 (Co_3O_4/graphene composites prepared using Triton X-100 and following by calcining precursors at 250 ℃) electrode. A specific capacitance of 494.2 F g^{-1} is exhibited at 7.2 Ag^{-1}, demonstrating appealing rate performance. After 1000 cycles, the specific capacitanceis 2.15 times of that of Co_3O_4/GNS-T-250 electrode, further demonstrates the great advantages as supercapacitors electrode.

Keywords: Supercapacitors, Graphene, Co_3O_4, Hydrothermal method

1. INTRODUCTION

Recently, supercapacitors have evoked increasing attention due to their superior power density, long cyclic life, and fast charge–discharge rate [1]. They have been applied in back-up power supplies, hybrid electric vehicles, and portable electronics [2]. Compared with carbon materials as electrodes in supercapacitors, transition metal oxides possess higher capacitance. Therefore, they have been widely investigated as electrode materials for supercapacitors [3-8]. Among transition metal oxides, Co_3O_4

occupies a very critical position because of environment safety, large theoretical specific capacitance, and favorable pseudocapacitive characteristics [9]. Ultralayered Co_3O_4 exhibited a specific capacitance of 548 F g^{-1} at 8 A g^{-1} [10]. 3D hierarchical Co_3O_4 twin-spheres displayed a specific capacitance of 781 F g^{-1} at 0.5 A g^{-1} [11]. A specific capacitance of 150 F g^{-1} at 1 A g^{-1} was obtained from porous Co_3O_4 particles [2]. We explored a chemical bath deposition method to synthesize Co_3O_4 thin film with a specific capacitance of 227 F g^{-1} at 0.2 A g^{-1} [3]. However, the specific capacitance of Co_3O_4 mentioned above is far below its theoretical specific capacitance of 3560 F g^{-1}. This is ascribable to the fact that relatively poor electron conductivity of Co_3O_4 results in ineffective electrochemical utilization.

To overcome disadvantages of Co_3O_4 mentioned above, carbon materials are employed to obtain Co_3O_4/carbon composites to improve the electric conductivity of Co_3O_4. Graphene is attractive in this regard because of its high electron conductivity, large specific surface area, superior intrinsic mechanical strength and chemical stability [12-14]. As a result, Co_3O_4/graphene composites for supercapacitors have attracted some research interests to obtain superior capacitive properties. Yan et al. synthesized Co_3O_4/graphene composites by microwave-assisted method [15]. Co_3O_4/graphene composites displayed higher specific capacitance (243.2 F g^{-1} at 10 mV s^{-1}) in comparison with pure graphene. Co_3O_4/graphene composites synthesized by a surfactant-assisted method showed a specific capacitance of 163.8 F g^{-1} at 1 A g^{-1}, which was about 13 times higher than that of pure Co_3O_4 [16]. The capacitive performance of Co_3O_4/graphene composites is superior to those of pure graphene and pure Co_3O_4 [15, 16], which is further confirmed by other researchers [17, 18]. Besides, Park et al. demonstrated effects of carbon blacks filler addition on capacitive performances of Co_3O_4/graphene composites [19]. Co_3O_4/graphene–carbon blacks (15 wt.%) showed the largest specific capacitance of 341 F g^{-1} at 10 mV s^{-1}. Guan et al. reported that the needle-like Co_3O_4/graphene composites exhibited a specific capacitance of 157.7 F g^{-1} at 0.1 A g^{-1} [14]. We previously demonstrated Co_3O_4/graphene composites with the specific capacitance of 703.4 F g^{-1} at 0.625 A g^{-1} [20]. However, the specific capacitance of Co_3O_4/graphene composites mentioned above is lower than expected specific capacitance and still need to be enhanced. Moreover, the literatures mentioned above about Co_3O_4/graphene composites for supercapacitors focused largely on selectivity of synthetic methods [15-20]. Up to now, there are no reports on influence of surfactant and calcining temperature on the morphology and size of Co_3O_4 in Co_3O_4/graphene composites, further affecting capacitive properties of Co_3O_4/graphene composites. Therefore, it is very necessary to carry out in-depth study in this field.

In the present work, the precursors are prepared by hydrothermal method with a mixed solution containing graphite oxide, cobalt nitrate, urea and trisodium citrate and surfactant. Then, Co_3O_4/graphene composites are obtained by calcining precursors at 250 ℃ and 350 ℃, respectively, and their capacitive behaviors are investigated. Electrochemical studies show that Co_3O_4/GNS-S-350 electrode possesses good capacitive behavior. Its specific capacitance at 0.2 A g^{-1} reaches 1033.4 F g^{-1}, which is much higher than those reported Co_3O_4/graphene composite electrodes in the literatures. Besides, it demonstrates appealing rate performance and the great advantages as supercapacitors electrode.

2. EXPERIMENTAL

2.1. Preparation and characterization of Co_3O_4/graphene composites

A modified Hummers method as described previously [20, 21] was used to synthesize graphite oxide. As-synthesized graphite oxide was immersed into 0.5 mol L^{-1} tetramethylammonium hydroxide (TMAOH) solution for a week. The brown dispersion was then dialyzed with deionized water until the pH equaled 7. After dialyzing, the brown dispersion dried in oven for 12 h at 60 ℃.

Co_3O_4/graphene composites were prepared by hydrothermal synthesis method as follows. The required amount of TMAOH-immersed graphite oxide was dispersed in 80 mL deionized water with sonication. Afterwards, Triton X-100 surfactant (0.64 mmol), $Co(NO_3)_2 \cdot 6H_2O$ (3.2 mmol), urea (6.4 mmol) and sodium citrate (0.64 mmol) were successively added to the above solution with stirring. The resulting solution was then transferred to a Teflon-lined autoclave of 100 mL capacity, followed by a thermal treatment at 150 ℃ for 24 h. After cooled, the obtained black precipitates at the bottom were washed thoroughly with deionized water by centrifugation and then dried in oven. Finally, the above black precipitates were calcined at 250 ℃ for 3 h. As a result, Co_3O_4/graphene composites, denoted as Co_3O_4/GNS-T-250, were obtained. The above black precipitates were calcinedat 350 ℃ under the same condition to obtain Co_3O_4/graphene composites, which were denoted as Co_3O_4/GNS-T-350.

The black precipitates were also prepared with a mixed solution including sodium dodecyl benzene sulfonate (SDBS) surfactant instead of Triton X-100 surfactant by the same procedure. Subsequently, the black precipitates were heated at 250 ℃ and 350 ℃ for 3 h, respectively. The obtained Co_3O_4/graphene composites were designated as Co_3O_4/GNS-S-250 and Co_3O_4/GNS-S-350, respectively.

The crystallographic structure of the synthesized composites was characterized by X-ray diffraction (XRD, Rigaku D/max 2550). The morphology of the composites was analyzed by scanning electron microscopy (SEM, FEI Nova Nano-230). Fourier-transform infrared (FT-IR) spectroscopy was recorded on a Nicolet 510P Fourier transformed infrared instrument.

2.2. Electrochemical measurements

A CHI 660D electrochemical workstation (Shanghai, China) was used to test electrochemical performance of the samples. Techniques of electrochemical measurements included cyclic voltammetry, chronopotentiometry, and electrochemical impedance spectroscopy. A three-electrode cell in 2M KOH solution was adopted in electrochemical measurements. The working electrodes were prepared as follows. A nickel foam (1 cm×1 cm) was used as current collector. The resultant composites (85 wt.%) as active materials, acetylene black (10 wt.%) as conductive agent, and poly(tetrafluoroethylene) (PTFE) as binder (5 wt.%) were mixed to form a slurry. Afterwards, the obtained slurry was pressed on current collector and dried under vacuum for 12 h at 110 °C. A platinum plate and a saturated calomel electrode (SCE) were used as the counter and reference

electrodes, respectively. Electrochemical impedance spectroscopy measurements were recorded in the frequency range from 0.01 to 10^5 Hz.

3. RESULTS AND DISCUSSION

3.1. XRD analyses

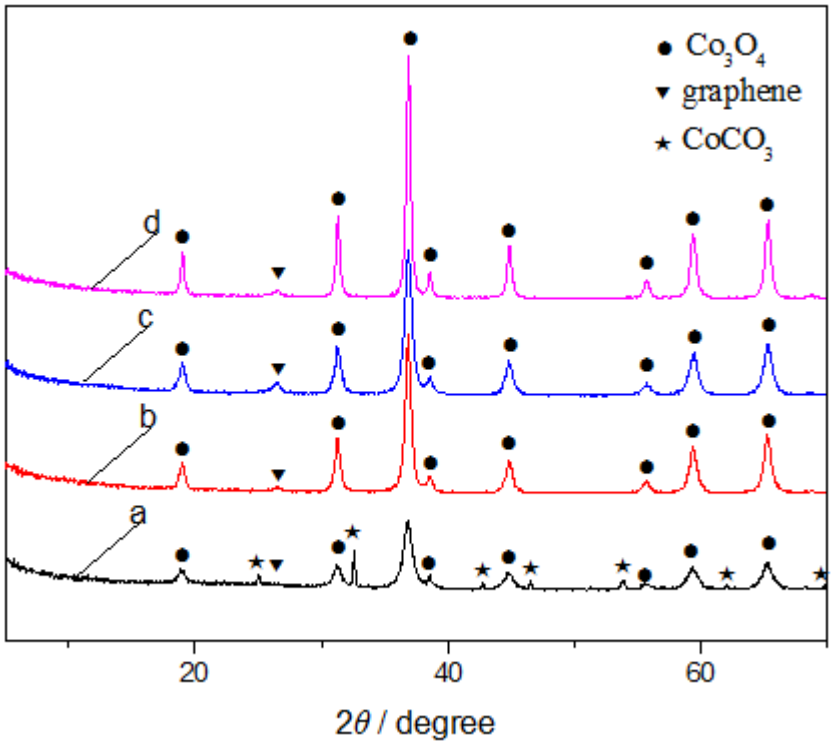

Figure 1. XRD patterns of Co_3O_4/GNS-S-250 (a), Co_3O_4/GNS-S-350 (b), Co_3O_4/GNS-T-250 (c) and Co_3O_4/GNS-T-350 (d).

Fig.1 presents XRD patterns of Co_3O_4/GNS-S-250, Co_3O_4/GNS-S-350, Co_3O_4/GNS-T-250 and Co_3O_4/GNS-T-350. As observed in curve a, the XRD peaks is indexed to Co_3O_4 (JCPDS No. 42-1476) and $CoCO_3$ (JCPDS No. 11-0692), together with characteristic peak at 26.5° attributed to the (002) plane of graphene [22]. It should be pointed out that $CoCO_3$ in Co_3O_4/GNS-S-250 is impurity. The XRD peaks of curve b are attributed to Co_3O_4 (JCPDS No. 42-1476) and graphene. The products obtained by calcining precursors at 250 ℃, which are synthesized with a mixed solution containing SDBS surfactant, contain Co_3O_4, graphene and $CoCO_3$. However, the products are the composites of Co_3O_4 and graphene when calcining temperature increases from 250 ℃ to 350 ℃. This clearly shows the complete decomposition of $CoCO_3$ to Co_3O_4 after calcined at 350 ℃. As shown in curves c and d, the XRD peaks are attributed to Co_3O_4 (JCPDS No. 42-1476) and graphene. This demonstrates that the products prepared by calcining the precursors at 250 ℃ and 350 ℃ synthesized with addition of Triton X-100 surfactant are the composites of Co_3O_4 and graphene. In addition, XRD patterns also show that different precursors are synthesized with different surfactants in the hydrothermal process.

The crystallite size of Co_3O_4 in Co_3O_4/GNS-S-250, Co_3O_4/GNS-S-350, Co_3O_4/GNS-T-250 and Co_3O_4/GNS-T-350 estimated by Scherrer formula with peak at 2θ =36.8° is 12.7, 17.2, 15.3 and 24.1 nm, respectively. This indicates that the crystallite size of Co_3O_4 in the composites calcined at 350 ℃ is larger than that of Co_3O_4 in the composites calcined at 250 ℃. Besides, compared with Co_3O_4 in the composites synthesized with addition of SDBS surfactant, Co_3O_4 in the composites prepared with addition of Triton X-100 surfactant exhibits larger crystallite size.

3.2. FT-IR spectra

To further support the XRD analyses, the FT-IR spectra of Co_3O_4/GNS-S-250 and Co_3O_4/GNS-T-250 are displayed in Fig. 2. In the literatures [20, 23], the intensive characteristic peaks of FT-IR spectrum of graphite oxide are at 3400 cm^{-1} and 1730 cm^{-1}, which are assigned to O-H stretching vibrations and C=O stretching vibrations of carboxyl groups, respectively.

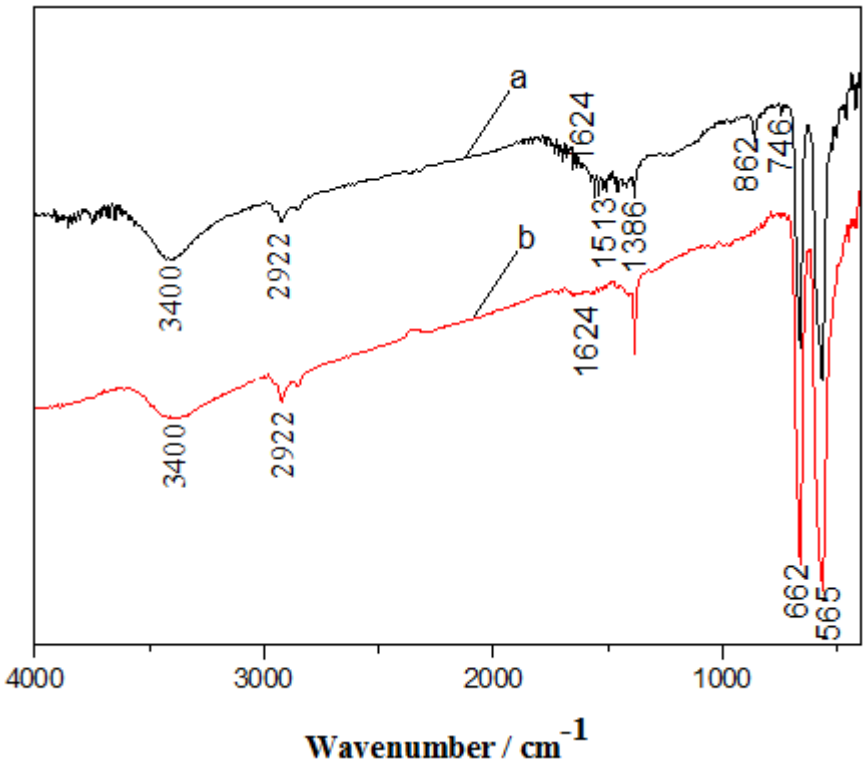

Figure 2. FT-IR spectra of Co_3O_4/GNS-S-250 (a) and Co_3O_4/GNS-T-250 (b).

As shown in Fig. 2, a decrease in intensity of the peak at 3400 cm^{-1} and the absence of the peak at 1730 cm^{-1} indicate that a lot of oxygen-containing groups of graphite oxide have been removed after reduction [24]. The peak at 1624 cm^{-1} is attributed to C=C skeletal vibrations of un-oxdized graphitic domains [25]. The peaks at 662 and 565 cm^{-1} are the characteristics of Co-O stretching vibrations in Co_3O_4 [26], indicating that the composites contain Co_3O_4. In addition, Co_3O_4/GNS-S-250 (curve a) contain OCO_2 stretching vibrations (1513 cm^{-1}) and CO_3^{2-} stretching vibrations (1386, 862 and 764

cm^{-1}) [27], revealing that $CoCO_3$ phase is detected in Co_3O_4/GNS-S-250. Thus, FT-IR results further confirm that Co_3O_4/GNS-S-350, Co_3O_4/GNS-T-250 and Co_3O_4/GNS-T-350 are the composites of Co_3O_4 and graphene. Whereas, Co_3O_4/GNS-S-250 are the composites of Co_3O_4, graphene and $CoCO_3$. This is consistent with results of XRD analyses.

3.3. Morphology

SEM images of Co_3O_4/GNS-S-250, Co_3O_4/GNS-S-350, Co_3O_4/GNS-T-250 and Co_3O_4/GNS-T-350 are shown in Fig. 3.

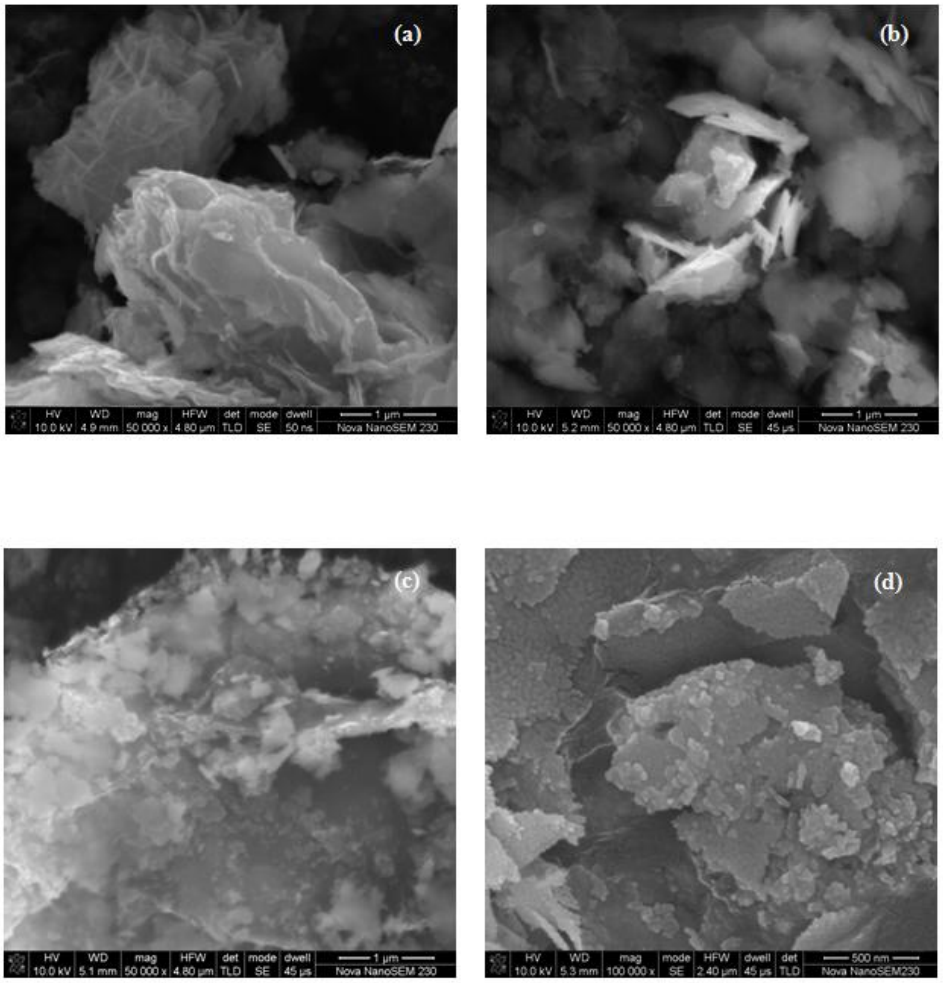

Figure 3.SEM of Co_3O_4/GNS-S-250(a), Co_3O_4/GNS-S-350 (b), Co_3O_4/GNS-T-250 (c) and Co_3O_4/GNS-T-350 (d).

As shown in Fig. 3, silk-like crumpled structure is graphene in the composites and nanoflake (a, b) or ellipsoidal-like nanoparticle (c, d) structure is Co_3O_4 in the composites. The morphology of Co_3O_4 in the composites synthesized with addition of SDBS surfactant consists of intercross nanoflakes with interspaces among them, indicating that the composites possess a high surface area when compared with ellipsoidal-like nanoparticle structure Co_3O_4 in the composites synthesized with

addition of Triton X-100 surfactant. Moreover, the crystallite size of Co_3O_4 in the composites fabricated with addition of SDBS surfactant is smaller than that of Co_3O_4 in the composites prepared with addition of Triton X-100 surfactant according to results of XRD analyses in Fig. 1. Therefore, Co_3O_4/GNS-S-250 and Co_3O_4/GNS-S-350 are more suitable for the penetration of electrolyte into the whole electrode material when compared with that of Co_3O_4/GNS-T-250 and Co_3O_4/GNS-T-350 [3, 28], exhibiting higher specific capacitance. XRD in Fig. 1 also presents the crystallite size of Co_3O_4 in the composites increases with the increase of calcining temperature. The increase in Co_3O_4 crystallite size is adverse to more active materials involved in redox reaction, resulting in reduction of the specific capacitance [29], indicating that the specificcapacitance of Co_3O_4/GNS-T-250 is higher than that of Co_3O_4/GNS-T-350. Compared with Co_3O_4/GNS-S-350, Co_3O_4 in Co_3O_4/GNS-S-250 composites exhibits smaller crystallite size. However, Co_3O_4/GNS-S-250 composites contain $CoCO_3$ impurity. Thus, we are not sure the specific capacitance of which is high in Co_3O_4/GNS-S-250 and Co_3O_4/GNS-S-350. Based on all the above reasons, capacitive properties of Co_3O_4/GNS-S-250, Co_3O_4/GNS-S-350 and Co_3O_4/GNS-T-250 are studied in the present paper.

3.4. Electrochemical capacitor property

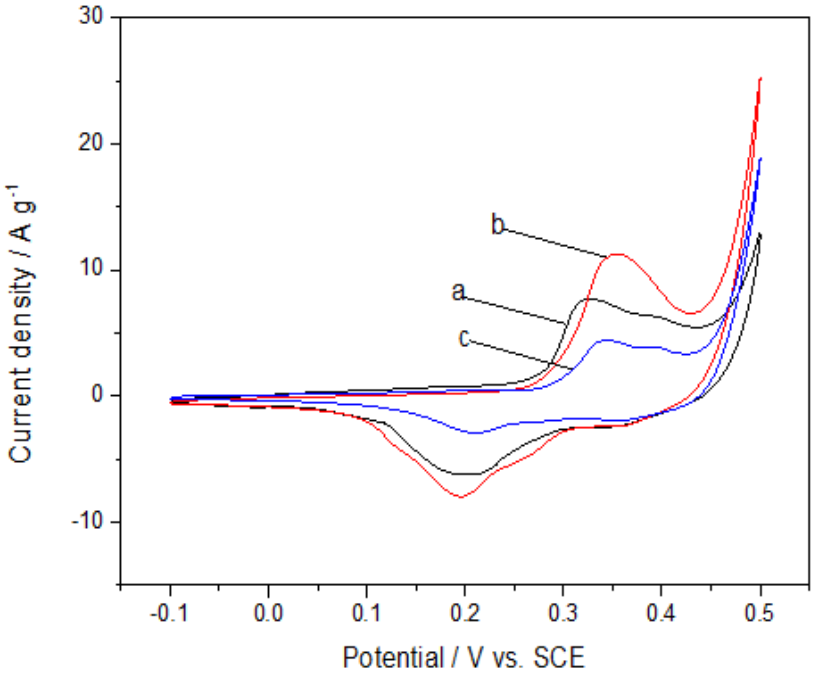

Figure 4. Cyclic voltammograms of Co_3O_4/GNS-S-250 electrode (a), Co_3O_4/GNS-S-350 electrode (b) and Co_3O_4/GNS-T-250 electrode (c) at a scan rate of 5 mV s^{-1}.

Fig. 4 demonstrates cyclic voltammograms Co_3O_4/GNS-S-250 electrode, Co_3O_4/GNS-S-350 electrode and Co_3O_4/GNS-T-250 electrode at a scan rate of 5mV s^{-1} in the potential window range from -0.1 to 0.5 V. The shape of cyclic voltammograms curves illustrates that the capacitance of the electrode is mainly considered into pseudocapacitance [30]. A detailed discussion about cyclic

voltammograms is referred to the literatures [31, 32]. There are anodic and cathodic peaks in the cyclic voltammograms curves. The redox peaks correspond to reactions as follows [3, 29, 32-35]:

$$CoOOH + OH^- \rightleftarrows CoO_2 + H_2O + e^- \quad (1)$$

$$Co_3O_4 + H_2O + OH^- \rightleftarrows 3CoOOH + e^- \quad (2)$$

As shown in Fig. 4, compared with Co_3O_4/GNS-S-250 electrode and Co_3O_4/GNS-T-250 electrode, Co_3O_4/GNS-S-350 electrode shows the largest current density and enclosed area within the potential scanning range, indicating that Co_3O_4/GNS-S-350 electrode possesses the highest specific capacitance. The main reason can be explained as follows. The morphology of Co_3O_4 in Co_3O_4/GNS-S-350 is composed of intercross nanoflakes with interspaces among them when compared with that of Co_3O_4 in Co_3O_4/GNS-T-250. This kind of structure of Co_3O_4 in Co_3O_4/GNS-S-350 can enhance the mass transportation and electrode conduction [36]. $CoCO_3$ phase is not detected in Co_3O_4/GNS-S-350, although the crystallite size of Co_3O_4 in Co_3O_4/GNS-S-350 is larger when compared with that of Co_3O_4 in Co_3O_4/GNS-S-250. As a result, the highest current density and enclosed area are displayed in Co_3O_4/GNS-S-350 electrode, and consequently the specific capacitance of Co_3O_4/GNS-S-350 electrode is highest among three electrodes.

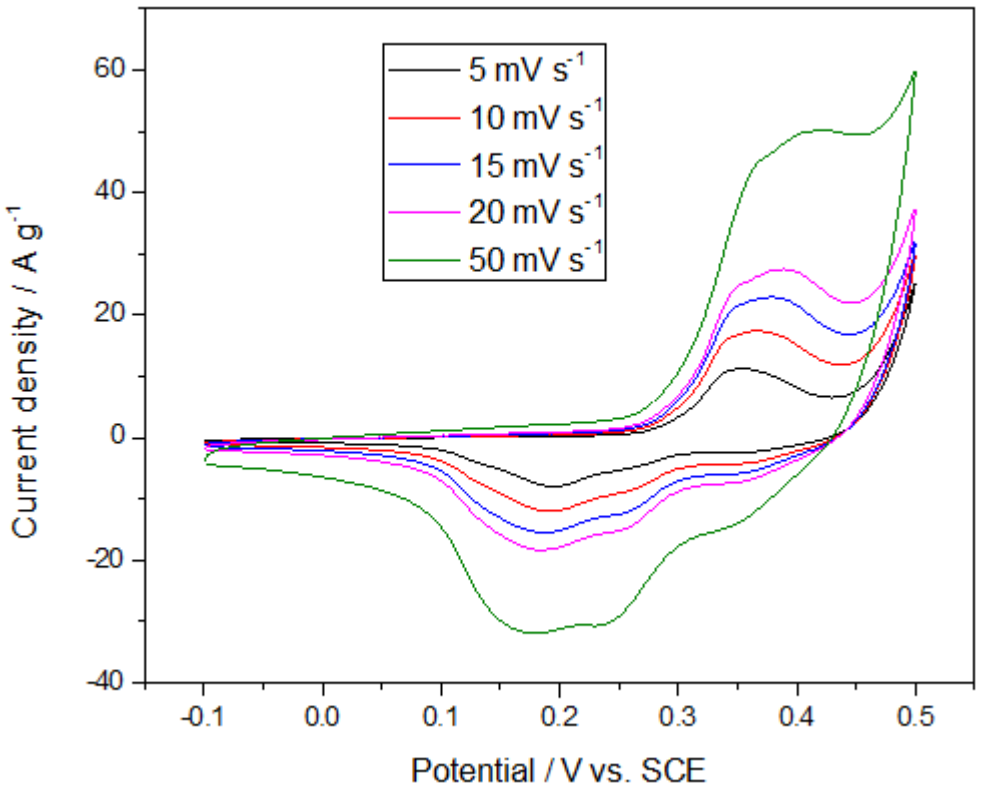

Figure 5. Cyclic voltammograms of Co_3O_4/GNS-S-350 electrode at scan rates of 5, 10, 15, 20 and 50 mV s^{-1}.

Fig. 5 depicts cyclic voltammograms of Co_3O_4/GNS-S-350 electrode at scan rates of 5, 10, 15, 20 and 50 mV s^{-1}. The anodic potential shifts to high value and the cathodic peak potential shifts to low value with the increase of scan rate, due to the limited diffusion time [37]. Besides, the peak

current densities increase with increasing scan rate, implying rapid redox reaction occurred among Co_3O_4/GNS-S-350 electrode [3, 35].

Fig. 6 shows galvanostatic charge–discharge curves of Co_3O_4/GNS-S-250 electrode, Co_3O_4/GNS-S-350 electrode and Co_3O_4/GNS-T-250 electrode at a current density of 1.4 A g^{-1} with in the potential range from 0 to 46 V. The crystallite size and the morphology of Co_3O_4 in the composites have great influence on the specific capacitance of composite electrodes. The specific capacitance of Co_3O_4/GNS-S-250 electrode, Co_3O_4/GNS-S-350 electrode and Co_3O_4/GNS-T-250 electrode can be calculated as follows [32, 38].

$$C_{sp} = \frac{I \times t}{V \times m} \tag{3}$$

where C_{sp}, I , t , V and m are the specific capacitance of composite electrodes, the discharge current, the discharge time, the discharge potential window and the mass of active material in composite electrodes, respectively.

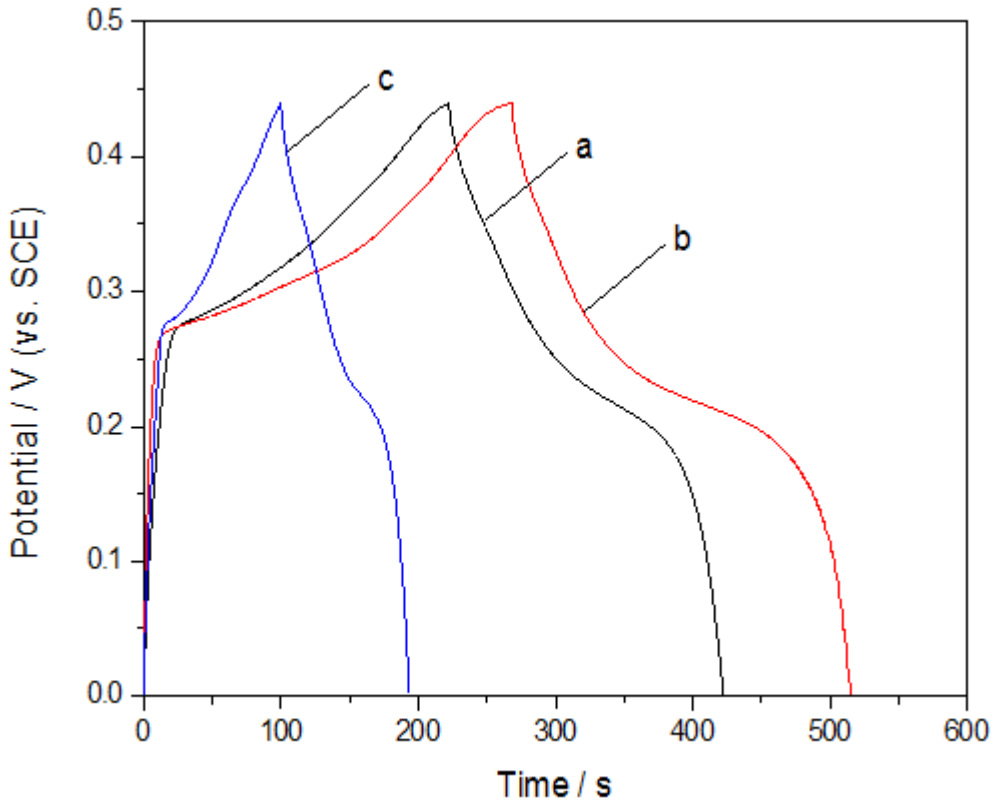

Figure 6. Galvanostatic charge–discharge curves of Co_3O_4/GNS-S-250 electrode (a), Co_3O_4/GNS-S-350 electrode (b) and Co_3O_4/GNS-T-250 electrode at a current density of 1.4 A g^{-1}.

As shown in Fig. 6, Co_3O_4/GNS-S-350 electrode exhibits the longest discharge time at the same current density, implying that its specific capacitance was the highest, which is consistent with results of cyclic voltammograms analyses. According to the equation (3), the specific capacitance of Co_3O_4/GNS-S-250 electrode, Co_3O_4/GNS-S-350 electrode and Co_3O_4/GNS-T-250 electrode are 636,

785.3 and 297 F g^{-1} at a current density of 1.4 A g^{-1}, respectively. Fig. 7 displays the specific capacitance calculated from equation (3) of Co_3O_4/GNS-S-250 electrode, Co_3O_4/GNS-S-350 electrode and Co_3O_4/GNS-T-250 electrode at the current densities of 0.2, 0.6, 1.0, 1.4, 1.8, 3.6, 5.4 and 7.2 A g^{-1}.

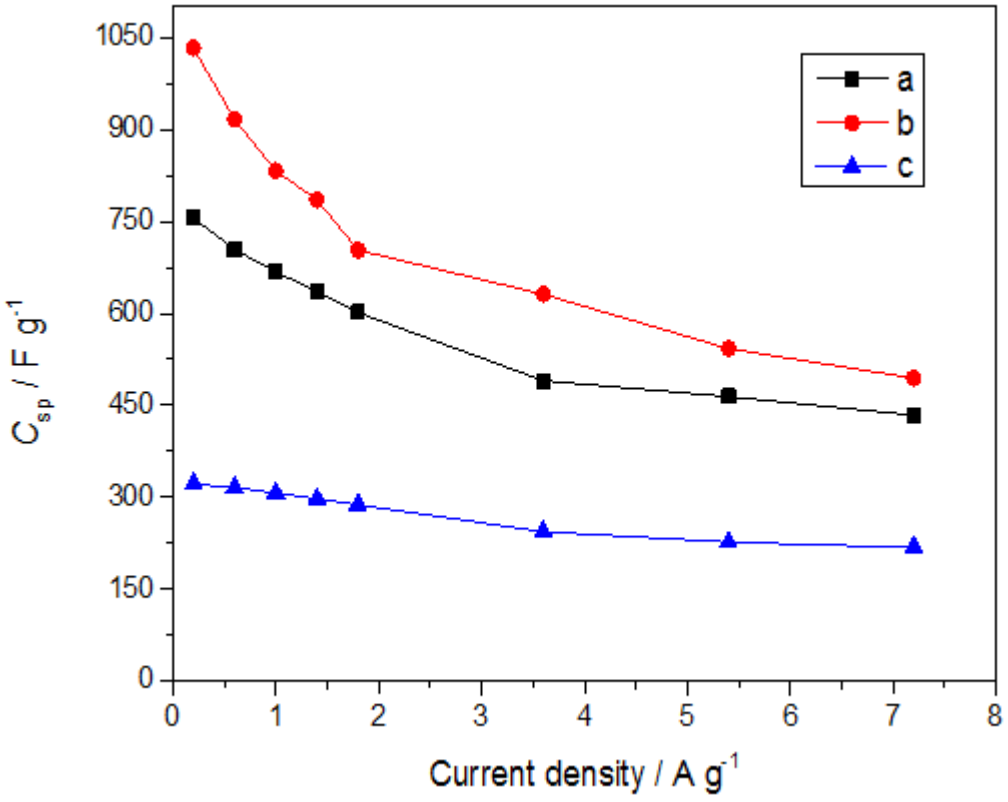

Figure 7. The calculated specific capacitance of Co_3O_4/GNS-S-250 electrode (a), Co_3O_4/GNS-S-350 electrode (b) and Co_3O_4/GNS-T-250 electrode (c) as a function of the current density.

As shown in Fig. 7, the specific capacitance of Co_3O_4/GNS-S-350 electrode is the highest at the same current density, the second is Co_3O_4/GNS-S-250 electrode, and Co_3O_4/GNS-T-250 electrode is the lowest. The specific capacitances of Co_3O_4/GNS-S-250 electrode, Co_3O_4/GNS-S-350 electrode and Co_3O_4/GNS-T-250 electrode at 0.2 A g^{-1} are 755.9, 1033.4 and 321.7 F g^{-1}, respectively. The specific capacitance of Co_3O_4/GNS-S-350 electrode at 0.2 A g^{-1} is 3.21 times of that of Co_3O_4/GNS-T-250 electrode. The reason of Co_3O_4/GNS-S-350 electrode with the highest specific capacitance at the same current density has been analyzed in results and discussion about cyclic voltammograms curves mentioned above. Fig. 7 also indicates that the composites synthesized with addition of SDBS exhibit higher specific capacitance than those synthesized with addition of Triton X-100. For Co_3O_4/GNS-S-350 electrode, a specific capacitance of 1033.4 F g^{-1} at 0.2 A g^{-1}, which is much larger than those reported Co_3O_4/graphene composite electrodes [14-18, 20, 22, 39]. The specific capacitance also reaches up to 832.4 F g^{-1} when the current density changes from 0.2 to 1.0 A g^{-1}. A

specific capacitance of 494.2 F g^{-1} is retained at 7.2 A g^{-1}, demonstrating appealing rate performance of Co_3O_4/GNS-S-350 as electrode materia for supercapacitors.

The long term stability of Co_3O_4/GNS-S-250 electrode, Co_3O_4/GNS-S-350 electrode and Co_3O_4/GNS-T-250 electrode is shown in Fig 8. For Co_3O_4/GNS-S-250 electrode, the specific capacitance slightly decreases from 490.1 to 472.6 F g^{-1} when the cycle number increases to 25 and then slightly increases to 495.3 F g^{-1} after 275 cycles. After 1000 cycles, a specific capacitance of 467.9 F g^{-1} is retained. In other words, the specific capacitance retention is 95.5% after 1000 cycles. As for Co_3O_4/GNS-S-350 electrode, the specific capacitance exhibits a relatively large decrease from 630.9 to 549.5 F g^{-1} after 25 cycles, which is due to the loss of active material during early cycle number [3, 40]. After 250 cycles, the specific capacitance slightly increases to 564.2 F g^{-1}, and then drop to 513.2 F g^{-1} after 1000 cycles. The specific capacitance retention is 81.3% after 1000 cycles. With regard to Co_3O_4/GNS-T-250 electrode, the specific capacitance remained stable on the whole with the increase of the cycle number. The initial specific capacitance of is calculated to be 243.9 F g^{-1}, and the specific capacitance is 238.5 F g^{-1} after 1000 cycles. The specific capacitance retention is 97.8% after 1000 cycles.

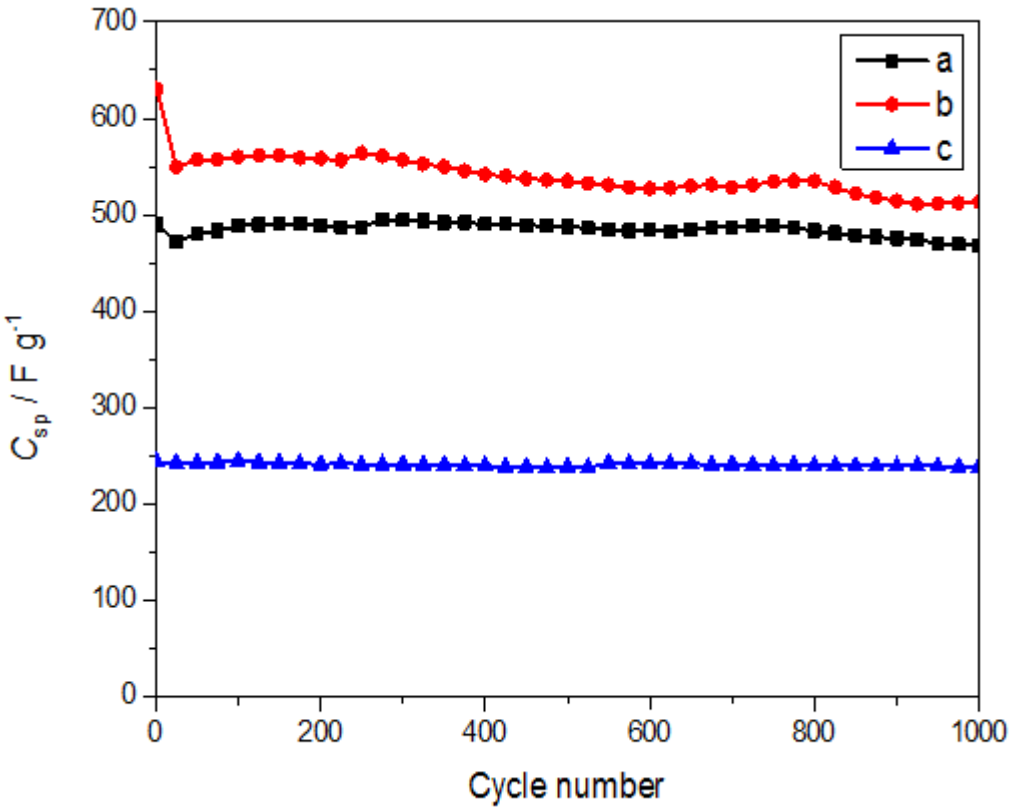

Figure 8. Cycling performance of Co_3O_4/GNS-S-250 electrode (a), Co_3O_4/GNS-S-350 electrode (b) and Co_3O_4/GNS-T-250 electrode (c) at a current density of 3.6 A g^{-1}.

Among three electrodes, the specific capacitance retention after 1000 cycles ranks in this order: Co_3O_4/GNS-T-250 electrode (97.8%), Co_3O_4/GNS-S-250 electrode (95.5%), Co_3O_4/GNS-S-350

electrode (81.3%). The reason of Co_3O_4/GNS-S-350 with the lowest specific capacitance retention has been analyzed mentioned above. Although Co_3O_4/GNS-S-350 electrode exhibits the lowest specific capacitance retention, the specific capacitance of Co_3O_4/GNS-S-350 electrode (513.2 F g^{-1}) after 1000 cycles is still the highest and 2.15 times of that of Co_3O_4/GNS-T-250 electrode (238.5 F g^{-1}). Such high specific capacitance at large current density after 1000 cycles further demonstrates the great advantages of Co_3O_4/GNS-S-350 as electrode material for supercapacitors.

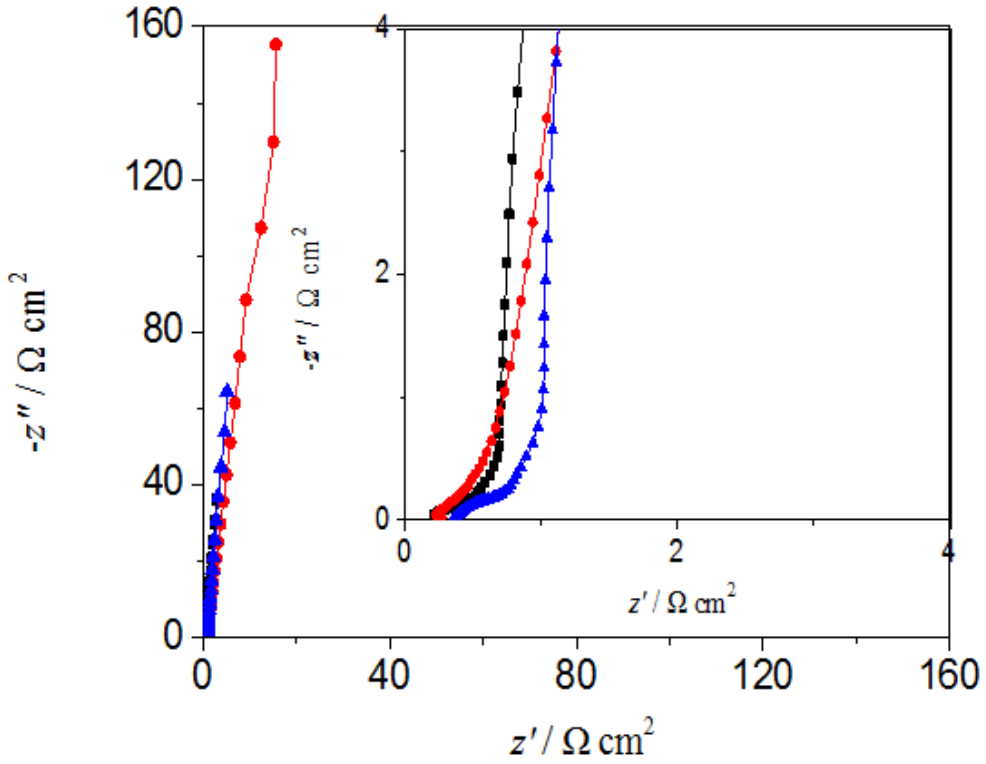

Figure 9. Nyquist plots of Co_3O_4/GNS-S-250 electrode (a), Co_3O_4/GNS-S-350 electrode (b) and Co_3O_4/GNS-T-250 electrode (c) measured at 0.1 V; The inset is the high frequency region.

Fig. 9 reveals Nyquist plots of Co_3O_4/GNS-S-250 electrode, Co_3O_4/GNS-S-350 electrode and Co_3O_4/GNS-T-250electrode. All Nyquist plots include two parts: a depressed semicircle component and a straight line component. The intersection of Nyquist plot at z' axis in the high frequency range is a combinational resistance (R_s) of ionic resistance of electrolyte, intrinsic resistance of the active material, and contact resistance at the active material/the current collector interface [41, 42]. This value is low because three composite electrodes all contain graphene with excellent electron conductivity. However, Co_3O_4/GNS-S-250 electrode and Co_3O_4/GNS-S-350 electrode show smaller R_s than Co_3O_4/GNS-T-250 electrode. Furthermore, a major difference is the semicircle in the high-frequency range, which arises from a parallel combination of the charge-transfer resistance (R_{ct}) and the double-layer capacitance (C_{dl}) [3, 14, 43]. It is clearly that the charge-transfer resistance increases in the order of Co_3O_4/GNS-S-350 electrode, Co_3O_4/GNS-S-250 electrode and Co_3O_4/GNS-T-250 electrode. The low charge-transfer resistance facilitates the high specific capacitance of the electrode. This means that

Co_3O_4/GNS-S-350 electrode possesses the highest specific capacitance, the second is Co_3O_4/GNS-S-250 electrode, and Co_3O_4/GNS-T-250 electrode is the lowest, which is in accordance with results from cyclic voltammograms curves in Fig. 4 and the specific capacitance in Fig. 7. The straight line of the low frequency range in Co_3O_4/GNS-S-250 electrode, Co_3O_4/GNS-S-350 electrode and Co_3O_4/GNS-T-250 electrode leans more towards z" axis.

4. CONCLUSIONS

Co_3O_4/graphene composites are obtained by hydrothermal synthesis method using different surfactants, followed by calcining precursors at different temperature. Different surfactants have a great influence on the crystallite size and the morphology of Co_3O_4 in the composites. The morphology of Co_3O_4 in the composites is intercross nanoflakes with interspaces among them and ellipsoidal-like nanoparticle by adding SDBS and Triton X-100 surfactants, respectively. Meanwhile, Co_3O_4 in the composites synthesized with addition of SDBS surfactant exhibits larger crystallite size than Co_3O_4 in the composites prepared with addition of Triton X-100 surfactant. The crystallite size increases with increasing calcining temperature from 250 ℃ to 350 ℃. The composites prepared in the presence of SDBS surfactant exhibit higher specific capacitance than those synthesized with addition of Triton X-100 surfactant. Among all the electrodes, Co_3O_4/GNS-S-350 electrode exhibits the highest specific capacitance. Its specific capacitance reaches 1033.4 F g^{-1} at 0.2 A g^{-1} and is 3.21 times of that of Co_3O_4/GNS-T-250 electrode, which is also much higher than those reported Co_3O_4/graphene composite electrodes. A specific capacitance of 494.2 F g^{-1} is retained at 7.2 Ag^{-1}, demonstrating appealing rate performance. After 1000 cycles, the specific capacitance retention is 81.3% and the specific capacitance (513.2 F g^{-1}) is 2.15 times of that of Co_3O_4/GNS-T-250 electrode (238.5 F g^{-1}), further demonstrates the great advantages of Co_3O_4/GNS-S-350 as supercapacitors electrode.

ACKNOWLEDGEMENTS
This work was financially supported by Science and Technology Plan Fund of Hunan Province (No. 2013GK3072), Scientific Research Fund of Hunan Provincial Education Department (No. 14B022) and Aid Program for Science and Technology Innovative Research Team in Higher Educational Institutions of Hunan Province.

References

1. Q. Zhang, E. Uchaker, S.L. Candelaria and G. Cao, *Chem. Soc. Rev.*, 42 (2013) 3127.
2. F.L. Meng, Z.G. Fang, Z.X. Li, W.W. Xu, M.J. Wang, Y.P. Liu, J. Zhang, W.R. Wang, D.Y. Zhao and X.H. Guo, *J. Mater. Chem. A*, 1 (2013) 7235.
3. Y.H. Li, K.L. Huang, Z.F. Yao, S.Q. Liu and X.X. Qing, *Electrochim. Acta*, 56 (2011) 2140.
4. Y.Q. Zhang, L. Li, S.J. Shi, Q.Q. Xiong, X.Y. Zhao, X.L. Wang, C.D. Gu and J.P. Tu, *J. Power Sources*, 256 (2014) 200.
5. Z.H. Yang, F.F. Xu, W.X. Zhang, Z.S. Mei, B. Pei and X. Zhu, *J. Power Sources*, 246 (2014) 24.
6. J.W. Xiao, S.X. Yang, L. Wan, F. Xiao and S. Wang, *J. Power Sources*, 245 (2014) 1027.
7. S.M. Chen, R. Ramachandran, V. Mani and R. Saraswathi, *Int. J. Electrochem. Sci.*, 9 (2014) 4072.
8. C.Y. Wan, L.Y. Yuan and H.Y. Shen, *Int. J. Electrochem. Sci.*, 9 (2014) 4024.
9. R.B. Rakhi, W. Chen, D.Y. Cha and H.N. Alshareef, *Nano Lett.*, 12 (2012) 2559.
10. S.K. Meher and G.R. Rao, *J. Phys. Chem. C*, 115 (2011) 15646.

11. Y. Xiao, S. Liu, F. Li, A. Zhang, J. Zhao, S. Fang and D. Jia, *Adv. Funct. Mater.*, 22 (2012) 4052.
12. M.F. El-Kady, V. Strong, S. Dubin and R.B. Kaner, *Science*, 335 (2012) 1326.
13. Y.W. Zhu, S. Murali, M.D. Stoller, K.J. Ganesh, W.W. Cai, P.J. Ferreira, A. Pirkle, R.M. Wallace, K.A. Cychosz, M. Thommes, D. Su, E.A. Stach and R.S. Ruoff, *Science*, 332 (2011) 1537.
14. Q. Guan, J.L. Cheng, B. Wang, W. Ni, G.F. Gu, X.D. Li, L. Huang, G.C. Yang and F.D. Nie, *ACS Appl. Mater. Interfaces*, 6 (2014) 7626.
15. J. Yan, T. Wei, W. Qiao, B. Shao, Q. Zhao, L. Zhang and Z. Fan, *Electrochim. Acta*, 55 (2010) 6973.
16. W.W. Zhou, J.P. Liu, T. Chen, K.S. Tan, X.T. Jia, Z.Q. Luo, C.X. Cong, H.P. Yang, C.M. Li and T. Yu, *Phys. Chem. Chem. Phys.*, 13 (2011) 14462.
17. H.W. Wang, Z.A. Hu, Y.Q. Chang, Y.L. Chen, Z.Y. Zhang, Y.Y. Yang and H.Y. Wu, *Mater. Chem. Phys.*, 130 (2011) 672.
18. B. Wang, Y. Wang, J. Park, H. Ahn and G.X. Wang, *J. Alloys Compd.*, 509 (2011) 7778.
19. S. Park and S. Kim, *Electrochim. Acta*, 89 (2013) 516.
20. X.W. Wang, S.Q. Liu, H.Y. Wang, F.Y. Tu, D. Fang and Y.H. Li, *J. Solid State Electrochem.*, 16 (2012) 3593.
21. W.S. Hummers and R.E. Offeman, *J. Am. Chem. Soc.*, 80 (1958) 1339.
22. D.H. Zhang and W.B. Zou, *Curr. Appl. Phys.*, 13 (2013) 1796.
23. Y. Wu, S. Liu, H. Wang, X. Wang, X. Zhang and G. Jin, *Electrochim. Acta*, 90 (2013) 210.
24. W. Zhang, W. He and X. Jing, *J. Phys. Chem. B*, 114 (2010) 10368.
25. C.Z. Yuan, L. Yang, L.R. Hou, J.Y. Li, Y.X. Sun, X.G. Zhang, L.F. Shen, X.J. Lu, S.L. Xiong and X.W. Lou, *Adv. Funct. Mater.*, 22 (2012) 2560.
26. F. Zhang, C.Z. Yuan, X.J. Lu, L.J. Zhang, Q. Che and X.G. Zhang, *J. Power Sources*, 203 (2012) 250.
27. X.H. Xia, J.P. Tu, Y.Q. Zhang, Y.J. Mai, X.L. Wang, C.D. Gu and X.B. Zhao, *Rsc Advances*, 2 (2012) 1835.
28. C.C. Hu, K.H. Chang, M.C. Lin and Y.T. Wu, *Nano Lett.*, 6 (2006) 2690.
29. Y.H. Li and Q.Y. Chen, *Asian J. Chem.*, 24 (2012) 4736.
30. M.S. Wu, C.Y. Huang and K.H. Lin, *J. Power Sources*, 186 (2009) 557.
31. C. Lin, J.A. Ritter and B.N. Popov, *J. Electrochem. Soc.*, 145 (1998) 4097.
32. Y.H. Li, K.L. Huang, D.M. Zeng, S.Q. Liu and Z.F. Yao, *J. Solid State Electrochem.*, 14 (2010) 1205.
33. N. Krstajic and S. Trasatti, *J. Electrochem. Soc.*, 142 (1995) 2675.
34. F. Švegl, B. Orel, M.G. Hutchins and K. Kalcher, *J. Electrochem. Soc.*, 143 (1996) 1532.
35. Y.H. Li, K.L. Huang, S.Q. Liu, Z.F. Yao and S.X. Zhuang, *J. Solid State Electrochem.*, 15 (2011) 587.
36. M. Nakayama, T. Kanaya and R. Inoue, *Electrochem. Commun.*, 9 (2007) 1154.
37. B.R. Duan and Q. Cao, *Electrochim. Acta*, 64 (2012) 154.
38. X. Yu, B. Lu and Z. Xu, *Adv. Mater.*, 26 (2014) 1044.
39. G.Y. He, J.H. Li, H.Q. Chen, J. Shi, X.Q. Sun, S. Chen and X. Wang, *Mater. Lett.*, 82 (2012) 61.
40. C.D. Lokhande, T.P. Gujar, V.R. Shinde, R.S. Mane and S.H. Han, *Electrochem. Commun.*, 9 (2007) 1805.
41. F.L. Luo, J. Li, Y. Lei, W. Yang, H.Y. Yuan and D. Xiao, *Electrochim. Acta*, 135 (2014) 495.
42. W.L. Yang, Z. Gao, J. Ma, J. Wang, B. Wang and L.H. Liu, *Electrochim. Acta*, 112 (2013) 378.
43. M.S. Wu and H.H. Hsieh, *Electrochim. Acta*, 53 (2008) 3427.

© 2015 The Authors. Published by ESG (www.electrochemsci.org). This article is an open access article distributed under the terms and conditions of the Creative Commons Attribution license (http://creativecommons.org/licenses/by/4.0/).